Letters in Applied NanoBioScience
Open-Access Journal (ISSN: 2284-6808)

Article
Volume 13, Issue 3, 2024, 120
https://doi.org/10.33263/LIANBS133.120

Systematic development of favipiravir lung targeted bio-nanoparticles

Hardik Rana [1*], Misba Vohra [1], Vimal Patel [2,*], Vaishali Thakkar [1]

[1] Department of Pharmaceutics, Anand Pharmacy College, Anand, Gujarat, India
[2] Department of Pharmaceutics, School of Pharmacy, P P Savani University, Surat, Gujarat, India
* Correspondence: email2vimal.patel@gmail.com (V.P.);

Scopus Author ID: 57212412830
Received: 16.05.2023; Accepted: 31.12.2023; Published: 26.07.2024

Abstract: A modified solvent evaporation process was used to produce polymeric nanoparticles containing favipiravir using the biodegradable polymer PLGA 50:50 and Poloxamer-407 as a hydrophilic surfactant. FTIR and DSC were used to examine the compatibility of drugs and polymers. Using a CCD model with two independent variables (PLGA and Poloxamer-407) and two dependent variables (percent encapsulation efficiency and particle size), QbD was able to identify and optimize the formulation-related parameters as well as those linked to the final product. The final optimized concentration of PLGA 50:50 was 190 mg, and Poloxamer-407 was 0.6%, confirmed by the validation of the design model. The generated favipiravir nanoparticles were characterized by DLS, zeta potential, aerodynamic size distribution, and *in-vitro* diffusion analysis. The optimized formulation's average particle size was roughly 270 nm, with excellent entrapment efficiency. Based on the zeta sizer, it was found that nanoparticles had a consistent spherical shape and good physical stability. *In-vitro* favipiravir release from an optimized formulation was sustained for up to 10 hrs. The biodegradable PLGA-based optimized nanoparticles loaded with favipiravir have become a promising COVID-19 therapeutic candidate.

Keywords: Favipiravir; PLGA 50:50; Poloxamer-407; CCD; Aerodynamic size distribution.

1. Introduction

The new severe acute respiratory syndrome coronavirus-2 (SARS-CoV-2) virus, which has been previously identified in humans, caused the unique Coronavirus disease (COVID-19) in late 2019. According to the WHO, there have been 632 million confirmed cases of COVID-19 worldwide as of 16 November 2022, with 6.5 million deaths [1]. There have been 43.8 million COVID-19 confirmed cases in India, with 0.52 million deaths [2,3]. The common symptoms of COVID-19 are trouble breathing, fever, and fatigue, while some elderly persons may not experience a fever as a symptom. Additional symptoms that could be present include aches and pains, runny nose, sore throat, and diarrhea [3]. Alveoli become inflamed (irritated and swollen) and fill with fluid as a result of the coronavirus, making breathing difficult. It causes an unbalanced amount of oxygen to be present in the body's blood [4]. The FDA has approved the use of antiviral drugs such favipiravir, remdesivir, lopinavir, ritonavir, dexamethasone, hydroxychloroquine, azithromycin, tocilizumab, etc., as first-line treatment for COVID-19 and therapies due to a public health emergency [5]. Remdesivir and favipiravir are the most effective drugs of all. Remdesivir is administered via intravenous (IV) infusion, although it comes with a number of side effects, including multiple organ failure and potential

toxicity in cardiovascular activities [6]. Additionally, the WHO observed that remdesivir had very little or no effect on the mortality rate in hospitalized COVID-19 patients [7].

Favipiravir belongs to a similar class; it can be taken orally. The active form of favipiravir inhibits viral genome replication by selectively inhibiting RNA polymerase. Favipiravir works well for mild to moderate stages. The primary barrier to the use of favipiravir is the large oral dose, which results in toxicity and limited bioavailability because it is less soluble and non-specific at the target location [8].

The prime inspiration of the present work is to design and evaluate lung-targeted PLGA nanoparticles loaded with favipiravir to address the drug's current issue with regard to increasing the bioavailability and effectiveness of the therapy. Prior studies have shown that PLGA nanoparticles increase solubility, reduce drug toxicity, and improve bioavailability [9]. They have been reported to provide controlled and sustained drug release, protect drugs from bursting before reaching the targeted site, and enhance intracellular penetration, in addition to their ability to facilitate drug delivery to the target site [10]. A hydrophilic non-ionic surfactant called poloxamer-407 was utilized to stabilize the hydrophobic PLGA nanoparticles in aqueous medium. By conducting a limited number of experiments, QbD is an approach that enables the investigation of multiple variables at once, their relationships, and their effects on various experimental responses. Additionally, mathematical models can determine the optimum number of variables needed for a certain response. The preparation of the favipiravir-loaded PLGA nanoparticles has been optimized well using the CCD. In order to examine the association between the experimental factors and the outcome and to obtain a suitable formulation, this method involved the analysis of 3-D response surfaces.

2. Materials and Methods

2.1. Materials

Favipiravir was received from the Zydus Research Centre in Ahmedabad as a gift sample. Merck in India provided the PLGA 50:50. Poloxamer-407 was acquired from Chemdys corporation in Ahmedabad. Excipients, solvents, and additional analytical-grade reagents were procured from S.D. Fine Chemicals in India.

2.2. Methods.

2.2.1. Drug identification and characterization.

Favipiravir drug characterization was carried out using UV-spectrophotometry (Shimadzu UV-1650 PC (E) 230V, Japan), FTIR (Perkin Elmer, Spectrum GX FTIR system), DSC (Perkin Elmer, Pyris-1 DSC), and melting point measurement utilizing capillary melting point apparatus [11].

2.2.2. Spectrophotometric analysis.

Using a UV-visible spectrophotometer with a 1 cm width quartz cell, the absorbance maxima (λmax) of serial dilution concentrations of favipiravir were measured in phosphate buffer (PBS) at pH 7.4 [12].

2.2.3. FTIR (Fourier transform infrared) spectroscopy.

FTIR was used to investigate the chemical interactions of favipiravir with PLGA and poloxamer-40. The accurate weight of the drug, polymer, surfactant, their physical mixture, and the formulation was weighed, and intimate the sample mixture was with KBr (1:10) using the solid dispersion method. All of the materials and mixes received IR radiation in the 400–4000 cm^{-1} range, and spectra were captured over the course of 16 cumulative scan cycles [13].

2.2.4. Differential Scanning Calorimetry (DSC).

DSC was used to examine how favipiravir physically interacted with PLGA and poloxamer-407 in this study. An aluminium sample pan was used to keep the exact weight of the drug, polymer, surfactant, their physical combination, and formulations. Aluminium covers were used to crimp-seal the pan. Under nitrogen flow, all samples were scanned at a uniform heating rate of 10°C/min between 50 and 300°C [14].

2.2.5. Preparation of nanoparticles.

We developed PLGA nanoparticles loaded with favipiravir by a modified solvent evaporation process employing a rotary evaporator and high-speed homogenization (HSH). In this procedure, the 50 mg of favipiravir and the 100 mg of PLGA (50:50) are dissolved in 10 ml of dichloromethane (DCM). Then, the required amount of surfactant (Poloxamer-407) is added to the resulting solution. The mixture is allowed to evaporate using a rotary evaporator at a temperature above their boiling point (50°C) and 80 rpm speed until a thin film is obtained at the bottom. The thin film was reconstituted with deionized water to produce a suspension of polymeric nanoparticles. The nanoparticles are homogenized in HSH for five minutes at a speed of 10,000 rpm. The nanoparticle suspensions were centrifuged at 3500 rpm for 60 min in 50 ml falcon tubes. The excess liquid was removed, and the remaining sample was pre-frozen for 24 hours at -22°C in a deep freezer. These frozen samples were freeze-dried for 72 hrs at 80°C and 1.0 bar at absolute vacuum pressure in a lyophilizer [15-18].

2.2.6. QbD and Risk assessment approach.

The Quality Target Product Profile (QTPP) was first developed while labeling specifications were taken into consideration. Critical Quality Attributes (CQAs) with a high likelihood of leading to product failure were found using Failure Mode Effect Analysis (FMEA) [19]. The initial phase in the risk assessment process was to evaluate every probable element that might have an effect on product quality. Based on a review of the literature, prior experiences, and results from early investigations of nanoformulation, these factors were organized hierarchically using an Ishikawa diagram, as shown in Figure 1. FMEA was used to describe the effects of specific failure modes. The severity of their impacts, or how frequently and easily they may be found, can be used to rank the modes of failure for risk management purposes using the FMEA method [20]. This information can be used to identify the CQA factors that need in-depth analysis and monitoring. An FMEA generates risk priority numbers (RPNs) for each combination of failure mode severity (S), occurrence (O), and detectability (D), which may be used to rank risk using the formula below [18,19].

$$\boldsymbol{RPN} = \begin{bmatrix}5\\4\\3\\2\\1\end{bmatrix} O \times \begin{bmatrix}5\\4\\3\\2\\1\end{bmatrix} S \times \begin{bmatrix}1\\2\\3\\4\\5\end{bmatrix} D \text{.....(1)}$$

The probability of an event happening, or its likelihood, was given a random score of 5, which indicates that it is highly likely to occur; 3, which indicates that it has a 50/50 chance of occurring; and 1, which indicates that it is highly unlikely to occur. S, the second parameter, assesses the impact on the system of a certain failure mode. Detectability, or how quickly a failure mode may be identified, is the final D parameter. A failure mode's risk to product quality decreases with ease of finding.

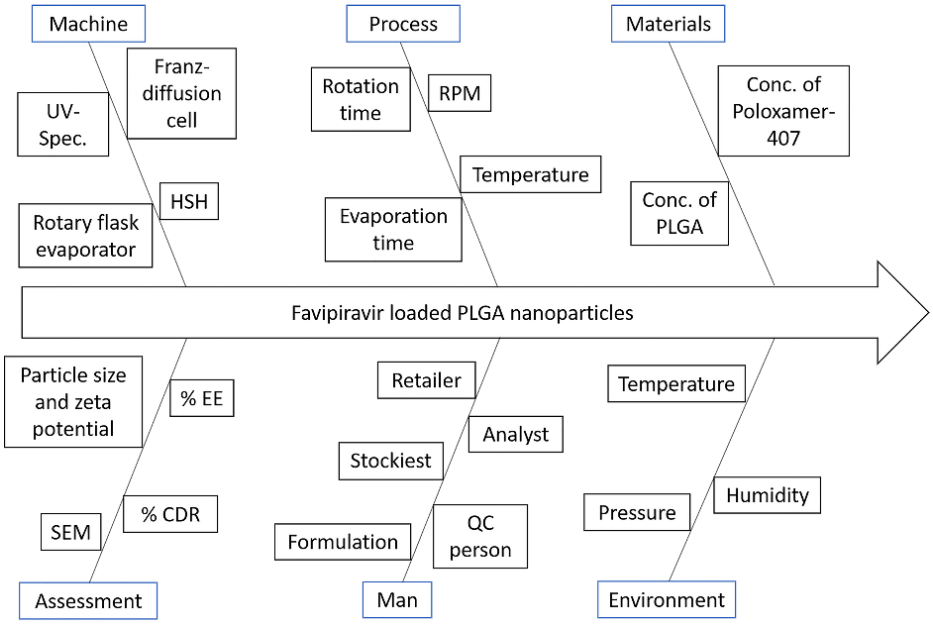

Figure 1. Ishikawa diagram.

2.2.7. Optimization of processing and product-related parameters using Central composite design (CCD).

CCD is widely used in response-surface modeling (RSM) for the optimization process. CCD is more robust than the Box-Behnken design because it has higher design points with a full quadratic model. A group of "star points" added to the embedded factorial or fractional factorial design in the CCD allows for the estimation of curvature. As indicated in Table 1, the amount of PLGA and poloxamer-407 was chosen as independent factors for the design, and the desired responses were particle size, percent encapsulation efficiency, and percent drug release at 10 hours. The PLGA nanoformulation was optimized using Design-Expert software v11.0.0. A total of 13 experimental runs were conducted based on the software, as shown in Table 2. The model was developed using multiple linear regression analysis (MLRA) and one-way ANOVA with a 0.05 probability (p) value for each dependent variable to be evaluated. The *p-value* was used to determine the parameter's significance. The terms with a higher *p-value* were removed for further investigation since they were deemed to be non-significant. Each measured response was given its own quadratic model, including with interactive and polynomial terms [20-22].

Table 1. Independent parameters and measured responses with their limits.

Independent variables	**Levels**					
	Coded values			**Actual values**		
	Low	Medium	High	Low	Medium	High
Conc. of PLGA 50:50 (mg)	-1	0	+1	50	100	150
Conc. of Poloxamer- 407 (%)	-1	0	+1	0.4	0.6	0.8
Dependent variables				**Limits (range)**		
Particle size (nm)				200-300		
Encapsulation efficiency (%)				70-90%		
Drug release at 10h (%)				More than 90%		

Table 2. Design matrix generated from Central-composite design.

Run order	**Actual values**		**%EE**	**Particle size (nm)**	**% CDR**
	PLGA Conc. (mg)	**Poloxamer-407 Conc. (%)**			
M1	50	0.8	83.78±0.24	168.8	99.03±0.47
M2	50	0.4	86.3±0.10	174.4	97.2±0.21
M3	170.711	0.6	97.9±.0.07	682.6	70.1±0.65
M4	150	0.8	95.6±0.14	373.5	79.9±0.84
M5	29.2893	0.8	88.5±0.05	161.9	100±0.39
M6	100	0.6	95.6±0.18	204.7	80±0.87
M7	100	0.882843	95.6±0.31	200	76.5±0.84
M8	150	0.4	88.5±0.25	424.7	74.2±0.52
M9	100	0.317157	83.7±0.33	242.8	81.5±0.46
M10	100	0.6	93.5±0.47	204.7	76.8±0.96
M11	100	0.6	95.6±0.11	204.7	82.4±0.55
M12	100	0.6	96.2±0.62	204.7	82±0.26
M13	100	0.6	95.1±0.64	204.7	84.1±0.33

2.2.8. Validation of statistical analysis for optimization.

Grid search analysis was used to verify the statistical model. One ideal composition and one checkpoint formulation were chosen from the optimized region using a random assessment approach. The checkpoint formulas were developed, taking into account various response factors. Each variable's experimental and predicted values were compared, and the % prediction error was computed beforehand [23,24].

2.2.9. % Entrapment efficiency (EE).

The solvent extraction method was used to calculate the entrapment efficiency. Dichloromethane: Methanol (1:9) solvent mixture was used to extract favipiravir from dried nanoparticles (equivalent to 2 mg of drug) using a vortex following centrifugation at 5000 rpm for 15 mins. The favipiravir-containing supernatant was tested for concentration using UV spectrophotometry after being adequately diluted with methanol. The % EE was calculated using the formula below [25-27].

$$\%\ \boldsymbol{Entrapment\ efficiency} = \frac{Drug\ content\ in\ nanoparticles}{Initial\ quantity\ of\ drug\ included}\ X\ 100 \text{.....(2)}$$

2.2.10. % Yield.

The percentage yield was calculated as the weight % of the final product after drying, with respect to the initial total amount of ingredients used for the preparations [28].

$$\%\ \boldsymbol{Yield} = \frac{Practical\ yield}{Theoritial\ yield}\ X\ 100 \text{.....(3)}$$

2.2.11. Particle size distribution.

The particle size of PLAG nanoparticles was determined using a Zetasizer Nano ZS90 (Malvern, UK). A 15 ml solution with 5 mg of nanoparticles in deionized water was prepared. A cuvette with a probe was used to contain the dispersion nanoparticle sample. Optical probes with coated windows are connected to the electrodes on the other side of an insulated sample cell. An electric field is used to create a connection between the optical probes and the appropriate electrodes. It is feasible to determine the particle size distribution from the velocity distribution of particles suspended in a dispersing media by applying the principles of dynamic light scattering. A graph of particle size distribution was produced using the flex software [27,29].

2.2.12. Zeta potential.

Zeta potential is an electrical charge that is present on the surface of nanoparticles and trades with the strength of the attraction between adjacent, equally charged nanomaterials, which raises questions regarding the materials' physical stability and aggregation potential [30]. Using a Zetasizer Nano ZS90 (Malvern, UK) at 25°C, the electrical potential on the surface of produced PLGA nanoparticles was measured. All samples were dispersed in deionized water/non-dissolving fluid 1 min prior to the analysis [31].

2.2.13. Aerodynamic behavior by Andersen cascade impactor.

The Andersen cascade impactor was used to conduct *in-vitro* lung diffusion of PLGA nanoparticles containing favipiravir (AN-200 Tokyo Dyrec, Japan). Eight perforated plates were arranged in ascending order of their diameter, starting with plate number “0” at the top and plate number 7 at the bottom. The base plate of each of these was connected to a vacuum with a flow rate of 28.3 l/min. Each of these had impact plates beneath it. An induction port was installed on the impactor's top. The dry powder inhaler with drug-loaded nanoparticles was attached to the device through a rubber collar. For a brief period, the vacuum pump operated

the device, and each plate's powdered nanoparticles were collected. Employing UV spectrophotometry, the drug concentration was determined after thoroughly washing each plate in distilled water. The % Respirable portion of the drug from stage 2 was calculated using the equation below [29,32].

$$\%\ \boldsymbol{Respirable\ fraction} = \frac{Amt.of\ drug\ deposited\ in\ lower\ stage}{Total\ drug\ dose}\ X\ 100 \text{.....(4)}$$

2.2.14. In-vitro diffusion study.

A dialysis tube with a molecular weight threshold of 12 kDa in a Franz diffusion cell, the *in-vitro* drug diffusion profile of nanoparticles carrying favipiravir was investigated. A 50 mg of favipiravir-containing nanoparticles were dissolved in 1 ml of PBS pH 7.4 and kept in the donor compartment. The receptor compartment was filled with 25 ml of PBS pH 7.4 and kept at 37°C under sink conditions for the duration of the diffusion research. Every two hours for ten hours, samples of about 1 ml were taken out with fresh media replacement to determine the amount of drug diffused using UV-spectrophotometry at a wavelength of 235 nm [30,33].

2.2.15. SEM.

The particle size, shape, and distribution of the optimized PLGA nanoparticles were measured using an SEM (ESEM/EDAX XL-30, Philips, Netherlands). Before SEM, the PLGA nanoparticles were lyophilized. The dried sample was mounted on the three-dimensionally rotated Eucentric goniometer stage while retained on an aluminum grid surface. The scanning was carried out in a nitrogen vacuum at a temperature of 25°C with a 30 kV accelerating voltage. The LaB6 filament was used to magnify the nanoparticles to a visible scale of 4,00,000 X (2 nm) [34].

2.2.16. Stability.

Powdered favipiravir-loaded PLGA nanoparticles were tested for six months in a controlled environment at 40°C and 75°RH to determine their short-term stability. In predetermine interval during a six-month particle size, % EE and % CDR of PLGA nanoparticles loaded with favipiravir were calculated [35].

3. Results and Discussion

3.1. Preparation of PLGA nanoparticle.

As previously mentioned, a modified solvent evaporation method was used to produce the favipiravir-loaded PLGA nanoparticles using a continuous phase system. To assess the drug entrapment behavior, polymerization, and size distribution pattern, preliminary screening of the polymers (PLGA 50:50 and PLA) and surfactants (Kolliphor- CS20, poloxamer-407, span-40, and Acconon) was conducted. According to the experimental findings, PLGA 50:50 has a lower particle size distribution and more drug entrapment than PLA. Meanwhile, poloxamer-407 stabilizes polymeric nanoparticles with uniform and narrow particle size distribution [36].

3.2. Identification of favipiravir.

A capillary melting point apparatus was used to determine the melting point of pure favipiravir API. The results demonstrated that the drug is naturally pure and devoid of any

impurities because the observed melting point (190°C) falls within the specified range (187-190°C). Figure 2 (a) illustrates the UV-spectrophotometry of favipiravir at serial dilution concentrations ranging from 20 to 100 g/ml in PBS pH 7.4. The drug showed a clear peak in absorbance at a wavelength of 235 nm and followed Beer's law within the dilution range. The linearity regression produced the equation Y = 0.0834X + 0.0068 with a r^2 value of 0.9994 [37].

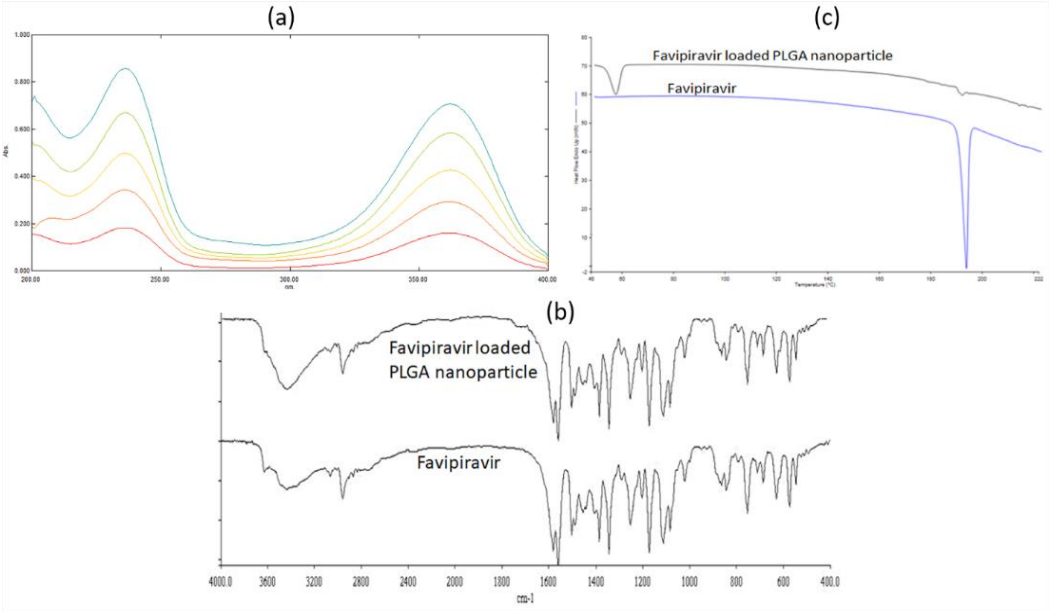

Figure 2. Identification of favipiravir: **(a)** UV- Spectrophotometry, drug-polymer compatibility studies, **(b)** FTIR, and **(c)** DSC.

3.3. Drug-polymer compatibility studies.

FITR spectroscopy was used to analyze the chemical interactions between favipiravir's surface functional groups and PLGA during the development of nanoformulations, which affect the drug's stability, bioavailability, and decomposition. Figure 2 (b) displays the FTIR data for favipiravir and PLGA nanoparticles containing the same. The characteristics of functional group peaks of favipiravir were seen in the formulation, respectively. Amorphism of the PLGA nanoparticles was seen to cause some peaks to disappear, as well as a little broadening of the peak intensity caused by the formation of a stable hydrogen bond. The result demonstrates that there was no incompatibility between PLGA and favipiravir in the nanoformulation. DSC carried out the physical interaction of favipiravir with PLGA. The thermograms of the drug and nanoformulations are illustrated in Figure 2 (c). The crystal structure of favipiravir was indicated by a prominent endothermic peak on the thermogram at 190°C, which corresponds to the melting point. Because the drug was completely dispersed in the nanoformulations, there was no obvious endothermic peak of the drug in the PLGA nanoparticle thermogram, confirming that the drug and polymer were not incompatible [31,32,35].

3.4. QbD & risk assessment.

The assessment of QTPPs for the formation of PLGA nanoparticles loaded with favipiravir is the first step of the QbD. The patient-centric QTPPs were identified based on the desired quality of the dosage form to accomplish targeted drug delivery. To achieve the desired profile, certain quality factors were identified. Tables 3 and 4 show polymeric nanoparticles'

acknowledged QTPPs and CQAs [38]. The RPN score using the FMEA technique for each parameter is calculated and listed in Table 5. According to Figure 1, the variables that affect the processing of polymeric nanoparticles were divided into the responses of the material, the worker, the measurement, the environment, the machine, and the process. Other than the material, the variables were thought to be low risk. With the help of early experiments and prior knowledge, these variables were all fixed to the same value. A high ranking was given to the parameters that show the impact on in-vivo product performance [39]. The significant effect on nanoparticle quality was determined using the RPN score for each variable. The RPN threshold was established at 60; values >60 were deemed critical, and lower values were not worthy of further investigation. As PLGA and poloxamer-407 had a major effect on both in-vivo and *in-vitro* performance, their concentration was considered significant [37,40].

Table 3. Selected QTTPs parameters.

Therapeutic Indication	**Pulmonary drug delivery**
Target Patient Population	Adults
Route of Administration	Pulmonary Administration
Site of Activity	Local Action in Lungs
Dosage form	Polymeric nanoparticles
Dose	50 mg

Table 4. Selected CQAs parameters.

Excipient (Quality Profile)	**Particle size & Morphology**
Particle Size	200-300nm
% Encapsulation efficiency	More than 90 %
Diffusion Study	Not less than 75% in 8 hr
Zeta Potential	-10 mV to -30 mV

Table 5. A summary of FMEA analysis.

	Variables	**Influence of variation**	**Occurrence**	**Itinerary of failure**	**Severity**	**Control Measure**	**Detection**	**RPN**	**Rank**
Material	The volume of organic solvent	Solubility of drug and formulation of nanoparticles	2	In different books, the ratio of two solvent	2	Volume measurement, quality of nanoparticles	2	8	8
	Concentration of Surfactant	**Stability, *In-vitro* drug release, Particle size, % EE**	**5**	**Variability in quality and quantity of material**	**5**	**Dissolution, strength, and % EE**	**5**	**125**	**1**
	Drug: Polymer ratio	**Stability, *In-vitro* drug release, Particle size, % EE**	**5**	**Variability in quality and quantity of material**	**5**	**Size determination, Dissolution, strength, and % EE**	**5**	**125**	**1**
Environment	Humidity	The overall quality of nanoparticles	1	Alteration in the condition of the atmosphere	1	Hygrometer	1	1	10

	Variables	Influence of variation	Occurrence	Itinerary of failure	Severity	Control Measure	Detection	RPN	Rank
	Pressure	No effect	1	Alteration in the shape of the atmosphere	1	Manometer	1	1	10
	Temperature	The overall quality of nanoparticles	1	Alteration in the state of the atmosphere	1	Thermometer or thermos-sensors	1	1	10
Man	Analyst	Testing of product	1	Physical error	1	Line clearance, Self-inspection, internal and external Audit, SOP	1	1	10
	Stockiest	Product Quality	1	Physica1 error	1	Proper storage and self-inspection	1	1	10
	Retailer	Product Quality	1	Physical error	1	Proper storage and self-inspection	1	1	10
	QC Person	Product quality testing	1	Physical error	1	Line clearance, Self-inspection, internal and external Audit, SOP	1	1	10
	Formulator	Product Quality	1	Physical error	1	Line clearance, Self-inspection, internal and external Audit, SOP	1	1	10
Measurement	**Particle size and size distribution**	**Stability and availability at the lower respiratory tract**	**5**	**No systematic development and failure of instrumentation**	**5**	**Malvern Zeta-sizer and Poly-dispersibility index**	**4**	**100**	**2**
	In-vitro drug release	Dissolution and therapeutic effect	4	No systematic development and failure of instrumentation	5	Franz diffusion cell	3	60	3
	Drug Loading	Dissolution and therapeutic effect	4	No systematic development and loss of instrumentation	5	Centrifugation	3	60	3
	% EE	**Therapeutic effect**	**4**	**No systematic development and failure of instrumentation**	**5**	**Centrifugation**	**5**	**100**	**2**
Machine	Franz Diffusion Cell	*In-vitro* drug release, IVIVC	4	The error of the analyst or instrument	3	Validation	3	36	5
	Rotary flask evaporator	The overall quality of nanoparticles	4	The error of the operator or instrument	5	Validation	5	100	10

	Variables	Influence of variation	Occurrence	Itinerary of failure	Severity	Control Measure	Detection	RPN	Rank
	Dryer	Physical property and stability	3	The mistake of the operator or instrument	1	Validation	1	3	9
Process	Rotation time	Physical properties of nanoparticles, % EE, and dissolution	3	The error of the operator or agent or Poor optimization of time	3	Optimization and validation of process	3	27	6
	Speed of Rotary flask evaporator (RPM)	Physical properties of nanoparticles, % EE, and dissolution	3	The error of the operator or instrument or Poor optimization of speed	3	Optimization and validation of process	3	27	6
	Temperature	Formation of thin film	3	The mistake of the operator or agent or Poor optimization of temperature	3	Optimization and validation of process	3	27	6
	Evaporation time	Formation of thin film	3	The error of the operator or instrument or Poor optimization of evaporation time	3	Optimization and validation of process	3	27	6
	Diameter of Rotary flask	Quality of nanoparticles	1	The error of the operator or instrument	1	Optimization and validation of process	1	1	10

3.5. Optimization of formulation using central composite design.

Using Design Expert software v11.0.0, a CCD was made in 13 operations of nanoparticle formulation. ANOVA and r^2 were used to validate the desired model fit summary. Based on the significance of the *p-value*, it was suggested that the Sequential Model Sum of Squares [Type-1] and model summary statistics were the models that best fit the design. The % EE, particle size and % CDR were measured in the experimental results.

Table 6. A summary of ANOVA results.

Source	% EE		Particle size (nm)		% CDR	
	F-value	***p*-value**	**F-value**	***p*-value**	**F-value**	***p*-value**
Model	6.57	0.0141	29.39	0.0001	11.90	0.0026
A-Conc. of PLGA	7.95	0.0258	85.07	< 0.0001	50.74	0.0002
B-Conc. of Poloxamer-407	9.68	0.0171	1.56	0.2521	0.0215	0.8874
AB	1.34	0.2843	0.0158	0.9036	0.8604	0.3845
A^2	1.21	0.3083	38.57	0.0004	5.37	0.0536
B^2	8.91	0.0204	0.1236	0.7355	0.0021	0.9644
Lack of Fit	15.84	0.0110			3.50	0.1288

Insignificant independent variables are those with a higher *p-value*, >0.05. In the first response, the *p-value* for Y1 was found to be 0.0069, which was significant, and the *p-value* for particle size was less than 0.0002, which was significant for all dependent variables, as shown in Table 6. The *p-value* for Y3 percent drug release was 0.0026, which was also significant [41].

3.5.1. Influence on % EE.

The % EE and the selected parameters have a good model fit, according to the r^2 Value (0.8244). The suggested quadratic model's significance was determined by its *p-value* of 0.0141. The findings imply that each independent variable has a major effect on the % EE. The *p-value* for % EE does not indicate any significance for the polynomial or interaction terms, so only the main effect of the relevant parameters can be used to draw conclusions. A *p-value* of 0.0258 indicated that the conc. of PLGA is significant. It follows logically that the % EE will rise as the amount of polymer increases. The *p-value* of 0.0171 indicated that conc. of poloxamer-407 was also significant. Figure 3's (a) contour plot and (b) 3D-RSM for the % EE provide greater context for the findings [35,42,43]. The % EE is expressed as a polynomial equation below:

$$\mathbf{Y = 94.94 + 3A + 3B + 1.48AB - 1.23\ A2 - 3.27B2.....(5)}$$

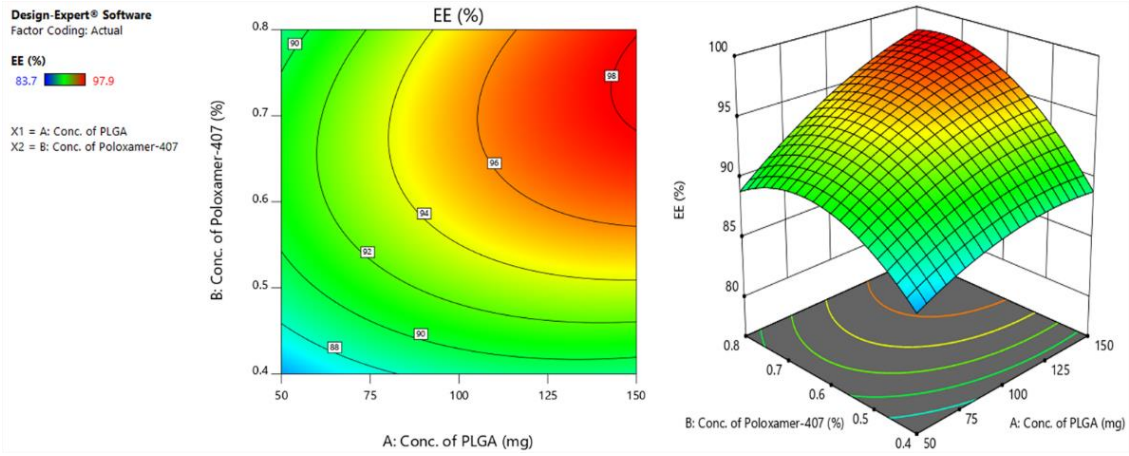

Figure 3. Contour plot and 3D-RSM of % EE.

3.5.2. Influence on particle size.

For particle size, the quadratic model gave an r^2 value of around 0.9545. Figure 4's (a) contour plot and (b) 3D-RSM showed that the only factor with a significant *p-value* of 0.0001 that would affect particle size was PLGA concentration. As PLGA concentration increased, so did particle size. While poloxamer-407 concentration was shown to get a higher *p-value* of 0.2521 with insignificant effects on particle size, increasing the concentration of both polymer and surfactant resulted in increased nanoparticles size [38,44]. Particle size is described below with a polynomial equation:

$$\mathbf{Y = 207.25 + 145.35A - 17.86B - 2.38AB + 102.96A^2 - 5.70B^2} \quad \mathbf{(6)}$$

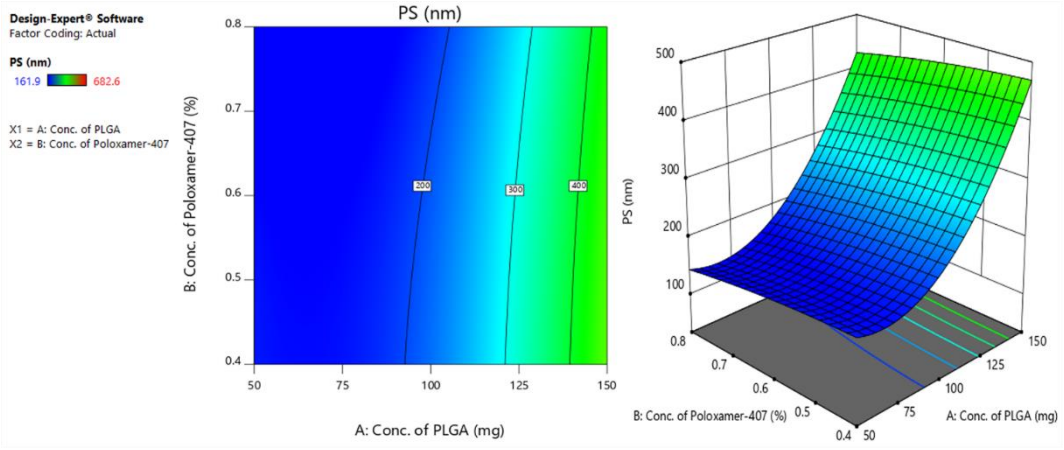

Figure 4. Contour plot and 3D-RSM of Particle size.

3.5.3. Influence on % Cumulative drug release.

The % CDR for the quadratic model provides an r^2 value of 0.8949. According to the results of Figure 5 (a) contour plot and (b) 3D-RSM and ANOVA, when PLGA concentration increased, the % CDR dropped with a *p-value* of 0.0002, whereas poloxamer-407 concentration had no significant effects on the % CDR, with a *p-value* of 0.8874. However, the combined effects of the two concentrations were found to reduce % CDR [41]. The following polynomial equation is suggested for the particle size:

$$\mathbf{Y = 81.27 – 10.92A – 0.2044B + 1.71AB + 3.74A^2 – 0.073B^2} \qquad \mathbf{(7)}$$

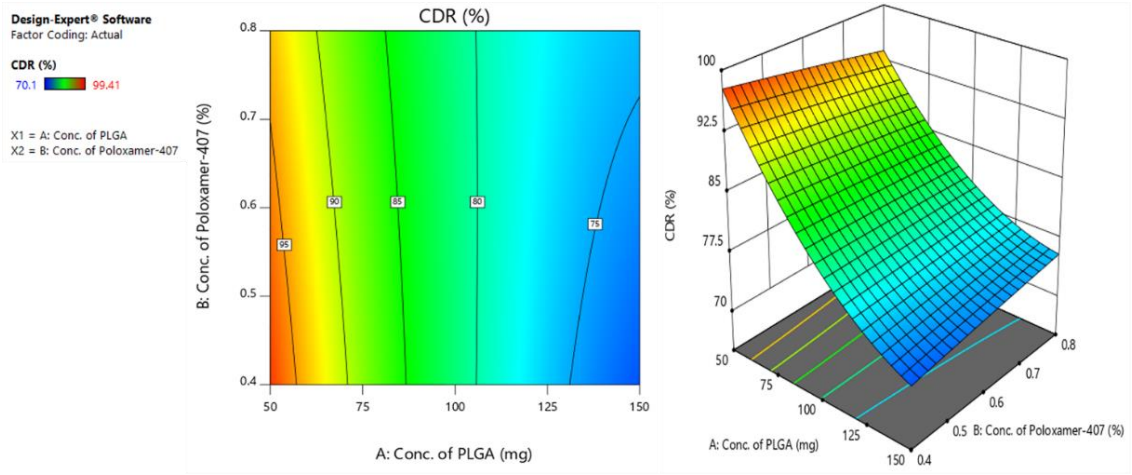

Figure 5. Contour plot and 3D-RSM of % CDR.

3.6. Characterization of optimized nanoparticle formulation.

3.6.1. Particle size distribution and zeta potential.

Particle size distribution, zeta potential, and polydispersity index were also evaluated for the prepared nanoparticles. An important parameter is particle size because it affects how drug molecules are delivered and targeted [45,46]. An average nanoparticle's median aerodynamic diameter for pulmonary drug delivery at the lowest region of the lungs is 200 nm. Figure 6 (a) shows a mean particle diameter of about 231 nm with a narrowed size distribution. As a result, the prepared PLGA nanoparticle is considered suitable for delivery to the lungs parenchyma. The zeta potential of drug-loaded PLGA nanoparticles was confirmed to be -16.8

mV with a variation of +16.8 mV in figure 6 (b), indicating that prepared nanoparticles have static electrical surface charges, which increase the physical stability by minimizing the aggregation inside the medium [41,47].

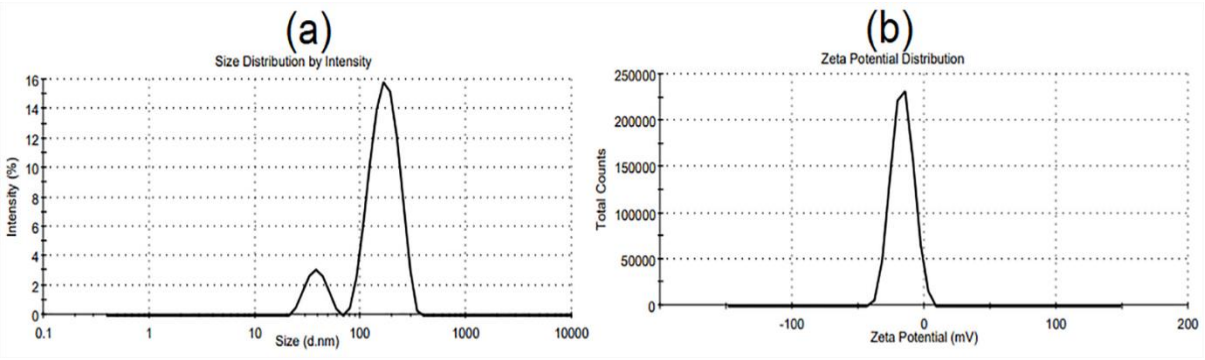

Figure 6. Characterization of optimized nanoparticles **(a)** Particle size distribution by DLS, **(b)** Zeta potential.

3.6.2. In-vitro diffusion study.

Figure 7 (a) showed that *in-vitro* drug release of optimized favipiravir-loaded PLGA nanoparticles was more than 90% within 10 hr of diffusion. A burst release of up to 40% of the drug was observed within 1 hr, which is influenced by solvent leaching, causing rapid phase inversion and slow hardening of the polymer, which causes porous nanoparticles. After that, from 2 hr completed, sustained drug release was reported till 12 hr of diffusion [48].

3.6.3. Aerodynamic behavior study using a cascade impactor.

An Andersen cascade impactor investigated the in-vitro lung diffusion and aerodynamic properties of favipiravir-loaded PLGA nanoparticles. The total amount of drug deposition was found to be 82%. The deposition percentages between each stage of the cascade impactor indicate % Respirable fraction, which is used to evaluate the possibility of delivering the nanoparticles to deep parts of the lung such as alveoli. The maximum amount of the drug concentration, 35%, has remained at stage 5 [32]. The % Respirable fraction was 86.44%, indicating the moderate aerosol performance of PLGA nanoparticles, as shown in Figure 7 (b).

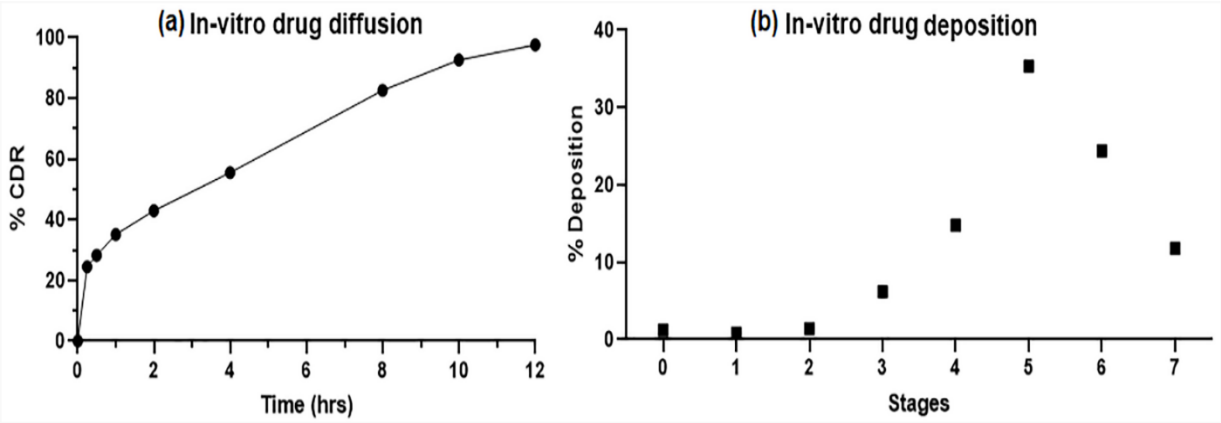

Figure 7. *In-vitro* assessment of optimized nanoparticles **(a)** *In-vitro* drug diffusion, **(b)** *In-vitro* drug deposition.

3.6.4. SEM.

The SEM images of pure favipiravir API and optimized PLGA nanoparticles loaded with the same are seen in Figure 8. The pure drug was obtained in the polymorphic state, and

an amorphous and aggregated drug structure was observed on the surface of larger cuboidal crystals, as seen in Figure 8 (a). Meanwhile, optimized nanoparticles were spherical in shape, had narrow size distribution, and had porous surfaces without any aggregation, as seen in Figure 8 (b).

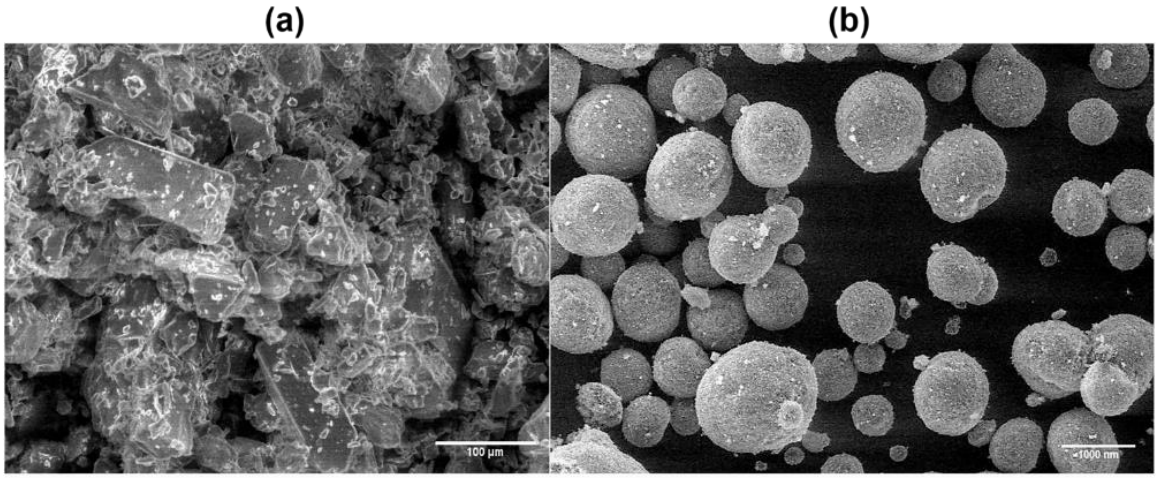

Figure 8. SEM images **(a)** favipiravir, **(b)** optimized nanoparticles.

3.6.5. Stability study.

The stability of optimized favipiravir containing PLGA nanoparticles was performed at 40±2ºC and 75±5% RH for six months. Table 7 shows particle size, % EE, and % CDR, which indicated that there was no significant variation observed after six months of storage [33,49].

Table 7. Stability of optimized batch of polymeric nanoparticles.

Time points (months)	Particle size (nm)	% EE	% CDR
0	225	99.32±0.25	92.17±0.69
1	254	96.67±0.74	91.88±058
2	247	91.21±0.63	91.28±0.63
4	248	90.78±0.52	90.67±0.21
6	258	91.76±0.11	92.99±0.47

4. Conclusions

The QbD approach was used to develop and design favipiravir-loaded PLGA nanoparticles successfully. The produced nanoparticles are promising for in-vivo site-specific lung targeting due to their narrow size distribution and high drug entrapment. The FTIR and DSC analyses showed that there were no drug-polymer interactions in the nanoparticle. The DLS and SEM revealed that PLGA nanoparticles have a uniform size distribution and a spherical shape without aggregation, verified by the nanoparticles' greater surface charges/zeta potential. The nanoparticles had a larger rate of lung deposition into the lower respiratory areas. The matrix polymeric system demonstrates favipiravir's sustainable and prolonged drug release pattern. As a result, the site-targeted delivery of favipiravir nanoformulation to the lungs could be an appropriate treatment regimen for managing COVID-19.

Funding

This research received no external funding.

Acknowledgments

Declared none.

Conflicts of Interest

The authors declare no conflict of interest.

References

1. World Health Organization. WHO Coronavirus Disease (COVID-19) Dashboard With Vaccination Data | WHO Coronavirus (COVID-19) Dashboard With Vaccination Data. World Health Organization. https://covid19.who.int/ (accessed 2022-11-17).
2. Government of India. #IndiaFightsCorona COVID-19 in India, Vaccination, Dashboard, Corona Virus Tracker | mygov.in. Government of India. https://www.mygov.in/covid-19 (accessed 2022-07-19).
3. Centre for Disease Prevention and Control (CDC). Symptoms of COVID-19 | CDC. Cdc. 2021.
4. Chavda, V.; Chaurasia, B.; Fiorindi, A.; Umana, G.E.; Lu, B.; Montemurro, N. Ischemic Stroke and SARS-CoV-2 Infection: The Bidirectional Pathology and Risk Morbidities. *Neurol. Int.* **2022**, *14*, 391–405, https://doi.org/10.3390/neurolint14020032.
5. National Institutes of Health. Antiviral therapy. COVID-19 Treatment Guidelines. Antiviral therapy. https://www.covid19treatmentguidelines.nih.gov/therapies/antiviral-therapy/ (accessed 2022-07-19).
6. FDA Updates. FDA Approves First Treatment for Erdheim-Chester Disease. *Oncol. Times* **2019**, *39*, 37-38, https://doi.org/10.1097/01.cot.0000528052.40878.44.
7. World Health Organization. Therapeutics and COVID-19 LIVING GUIDELINE. World Health Organisation. https://www.who.int/publications/i/item/WHO-2019-nCoV-therapeutics-2022.4 (accessed 2022-07-19).
8. Agrawal, U.; Raju, R.; Udwadia, Z.F. Favipiravir: A new and emerging antiviral option in COVID-19. *Med. J. Armed Forces India* **2020**, *76*, 370–376, https://doi.org/10.1016/j.mjafi.2020.08.004.
9. Heidari, M.; Salmanpour, M.; Tamaddon, A.-M. Implication of nanotechnology-based approaches to combat SARS-CoV-2 infection. *Indian J. Pharmacol.* **2021**, *53*, 78-79, https://doi.org/10.4103/IJP.IJP_857_20.
10. Charelli, L.E.; de Mattos, G.C.; de Jesus Sousa-Batista, A.; Pinto, J.C.; Balbino, T.A. Polymeric nanoparticles as therapeutic agents against coronavirus disease. *J. Nanopart. Res.* **2022**, *24*, 12, https://doi.org/10.1007/s11051-022-05396-5.
11. Pinto, M.; Silva, V.; Barreiro, S.; Silva, R.; Remião, F.; Borges, F.; Fernandes, C. Brain drug delivery and neurodegenerative diseases: Polymeric PLGA-based nanoparticles as a forefront platform. *Ageing Res. Rev.* **2022**, *79*, 101658, https://doi.org/10.1016/j.arr.2022.101658.
12. Nair, A.B.; Al-Dhubiab, B.E.; Shah, J.; Vimal, P.; Attimarad, M.; Harsha, S. Development and evaluation of palonosetron loaded mucoadhesive buccal films. *J. Drug Deliv. Sci. Technol.* **2018**, *47*, 351–358, https://doi.org/10.1016/j.jddst.2018.08.014.
13. Salatin, S.; Barar, J.; Barzegar-Jalali, M.; Adibkia, K.; Alami-Milani, M.; Jelvehgari, M. Formulation and Evaluation of Eudragit RL-100 Nanoparticles Loaded in-Situ Forming Gel for Intranasal Delivery of Rivastigmine. *Adv. Pharm. Bull.* **2020**, *10*, 20–29, https://doi.org/10.15171/apb.2020.003.
14. Nanaki, S.G.; Spyrou, K.; Bekiari, C.; Veneti, P.; Baroud, T.N.; Karouta, N.; Grivas, I.; Papadopoulos, G.C.; Gournis, D.; Bikiaris, D.N. Hierarchical Porous Carbon—PLLA and PLGA Hybrid Nanoparticles for Intranasal Delivery of Galantamine for Alzheimer's Disease Therapy. *Pharmaceutics* **2020**, *12*, 227, https://doi.org/10.3390/pharmaceutics12030227.
15. Hu, X.; Han, R.; Quan, L.-H.; Liu, C.-Y.; Liao, Y.-H. Stabilization and sustained release of zeylenone, a soft cytotoxic drug, within polymeric micelles for local antitumor drug delivery. *Int. J. Pharm.* **2013**, *450*, 331–337, https://doi.org/10.1016/j.ijpharm.2013.04.007.
16. Szczęch, M.; Szczepanowicz, K. Polymeric Core-Shell Nanoparticles Prepared by Spontaneous Emulsification Solvent Evaporation and Functionalized by the Layer-by-Layer Method. *Nanomaterials* **2020**, *10*, 496, https://doi.org/10.3390/nano10030496.
17. Jia, F.; Li, Y.; Lu, J.; Deng, X.; Wu, Y. Amphiphilic Block Copolymers-Guided Strategies for Assembling Nanoparticles: From Basic Construction Methods to Bioactive Agent Delivery Applications. *ACS Appl. Bio Mater.* **2020**, *3*, 6546–6555, https://doi.org/10.1021/acsabm.0c01039.

18. Hernández-Giottonini, K.Y.; Rodríguez-Córdova, R.J.; Gutiérrez-Valenzuela, C.A.; Peñuñuri-Miranda, O.; Zavala-Rivera, P.; Guerrero-Germán, P.; Lucero-Acuña, A. PLGA nanoparticle preparations by emulsification and nanoprecipitation techniques: effects of formulation parameters. *RSC Adv.* **2020**, *10*, 4218–4231, https://doi.org/10.1039/c9ra10857b.
19. Schneider, H. Failure Mode and Effect Analysis: FMEA from Theory to Execution. *Technometrics* **1996**, *38*, 80, https://doi.org/10.2307/1268911.
20. Fahmy, R.; Kona, R.; Dandu, R.; Xie, W.; Claycamp, G.; Hoag, S.W. Quality by Design I: Application of Failure Mode Effect Analysis (FMEA) and Plackett-Burman Design of Experiments in the Identification of "Main Factors" in the Formulation and Process Design Space for Roller-Compacted Ciprofloxacin Hydrochloride Immediat. *AAPS PharmSciTech* **2012**, *13*, 1243–1254, https://doi.org/10.1208/s12249-012-9844-x.
21. Mahdizadeh, M.; Zamanzade, E. A new reliability measure in ranked set sampling. *Stat. Papers* **2018**, *59*, 861–891, https://doi.org/10.1007/s00362-016-0794-3.
22. Zamanzade, E.; Mahdizadeh, M. Using ranked set sampling with extreme ranks in estimating the population proportion. *Stat. Methods Med. Res.* **2020**, *29*, 165–177, https://doi.org/10.1177/0962280218823793.
23. Oz, U.C.; Küçüktürkmen, B.; Devrim, B.; Saka, O.M.; Bozkir, A. Development and Optimization of Alendronate Sodium Loaded PLGA Nanoparticles by Central Composite Design. *Macromol. Res.* **2019**, *27*, 857–866, https://doi.org/10.1007/s13233-019-7119-z.
24. Saka, O.M.; Öz, U.C.; Küçüktürkmen, B.; Devrim, B.; Bozkır, A. Central Composite Design for Optimization of Zoledronic Acid Loaded PLGA Nanoparticles. *J. Pharm. Innov.* **2020**, *15*, 3–14, https://doi.org/10.1007/s12247-018-9365-6.
25. Cortés, H.; Hernández-Parra, H.; Bernal-Chávez, S.A.; Del Prado-Audelo, M.L.; Caballero-Florán, I.H.; Borbolla-Jiménez, F.V.; González-Torres, M.; Magaña, J.J.; Leyva-Gómez, G. Non-Ionic Surfactants for Stabilization of Polymeric Nanoparticles for Biomedical Uses. *Materials* **2021**, *14*, 3197, https://doi.org/10.3390/ma14123197.
26. Gurram, R.K.; Gandra, S.; Shastri, N.R. Design and Optimization of Disintegrating Pellets of MCC by Non-Aqueous Extrusion Process Using Statistical Tools. *Eur. J. Pharm. Sci.* **2016**, *84*, 146–156, https://doi.org/10.1016/j.ejps.2016.01.021.
27. Badaoui, F.Z.; Bouzid, D. Formulation and Optimization of Diclofenac Sodium Loaded Ethylcellulose Nanoparticles. *Braz. J. Pharm. Sci.* **2022**, *58*, 2022, https://doi.org/10.1590/S2175-97902022E19586.
28. Bhatt, K.; Patil, P.; Jani, P.; Thakkar, P.; Sawant, K. Design and evaluation of hyaluronic acid-coated PLGA nanoparticles of raloxifene hydrochloride for treatment of breast cancer. *Drug Dev. Ind. Pharm.* **2022**, *47*, 2013–2024, https://doi.org/10.1080/03639045.2022.2088784.
29. Bhanderi, M.; Shah, J.; Gorain, B.; Nair, A.B.; Jacob, S.; Asdaq, S.M.B.; Fattepur, S.; Alamri, A.S.; Alsanie, W.F.; Alhomrani, M.; Nagaraja, S.; Anwer, M.K. Optimized Rivastigmine Nanoparticles Coated with Eudragit for Intranasal Application to Brain Delivery: Evaluation and Nasal Ciliotoxicity Studies. *Materials* **2021**, *14*, 6291, https://doi.org/10.3390/ma14216291.
30. Song, X.; Zhao, Y.; Hou, S.; Xu, F.; Zhao, R.; He, J.; Cai, Z.; Li, Y.; Chen, Q. Dual agents loaded PLGA nanoparticles: Systematic study of particle size and drug entrapment efficiency. *Eur. J. Pharm. Biopharm.* **2008**, *69*, 445–453, https://doi.org/10.1016/j.ejpb.2008.01.013.
31. Asal, H.A.; Shoueir, K.R.; El-Hagrasy, M.A.; Toson, E.A. Controlled synthesis of *in-situ* gold nanoparticles onto chitosan functionalized PLGA nanoparticles for oral insulin delivery. *Int. J. Biol. Macromol.* **2022**, *209*, 2188–2196, https://doi.org/10.1016/j.ijbiomac.2022.04.200.
32. Rawal, T.; Parmar, R.; Tyagi, R.K.; Butani, S. Rifampicin loaded chitosan nanoparticle dry powder presents an improved therapeutic approach for alveolar tuberculosis. *Colloids Surfaces B Biointerfaces* **2017**, *154*, 321–330, https://doi.org/10.1016/j.colsurfb.2017.03.044.
33. Nair, A.B.; Shah, J.; Al-Dhubiab, B.E.; Patel, S.S.; Morsy, M.A.; Patel, V.; Chavda, V.; Jacob, S.; Sreeharsha, N.; Shinu, P.; Attimarad, M.; Venugopala, K.N. Development of Asialoglycoprotein Receptor-Targeted Nanoparticles for Selective Delivery of Gemcitabine to Hepatocellular Carcinoma. *Molecules* **2019**, *24*, 4566, https://doi.org/10.3390/molecules24244566.
34. Sun, Y.; Bhattacharjee, A.; Reynolds, M.; Li, Y.V. Synthesis and characterizations of gentamicin-loaded poly-lactic-co-glycolic (PLGA) nanoparticles. *J. Nanoparticle Res.* **2021**, *23*, 115, https://doi.org/10.1007/s11051-021-05293-3.
35. Elbatanony, R.S.; Parvathaneni, V.; Kulkarni, N.S.; Shukla, S.K.; Chauhan, G.; Kunda, N.K.; Gupta, V. Afatinib-loaded inhalable PLGA nanoparticles for localized therapy of non-small cell lung cancer

(NSCLC)—development and in-vitro efficacy. *Drug Deliv. Transl. Res.* **2021**, *11*, 927–943, https://doi.org/10.1007/s13346-020-00802-8.
36. Ahmad, M.Z.; Sabri, A.H.B.; Anjani, Q.K.; Domínguez-Robles, J.; Abdul Latip, N.; Hamid, K.A. Design and Development of Levodopa Loaded Polymeric Nanoparticles for Intranasal Delivery. *Pharmaceuticals* **2022**, *15*, 370, https://doi.org/10.3390/ph15030370.
37. Tulbah, A.S.; Lee, W.-H. Physicochemical Characteristics and in Vitro Toxicity/Anti-Sars-Cov-2 Activity of Favipiravir Solid Lipid Nanoparticles (SLNs). *Pharmaceuticals* **2021**, *14*, 1059, https://doi.org/10.3390/ph14101059.
38. Németh, Z.; Pallagi, E.; Dobó, D.G.; Kozma, G.; Kónya, Z.; Csóka, I. An Updated Risk Assessment as Part of the QbD-Based Liposome Design and Development. *Pharmaceutics* **2021**, *13*, 1071, https://doi.org/10.3390/pharmaceutics13071071.
39. Kozaki, M.; Kobayashi, S.-i.; Goda, Y.; Okuda, H.; Sakai-Kato, K. Evaluating the Properties of Poly(Lactic-Co-Glycolic Acid) Nanoparticle Formulations Encapsulating a Hydrophobic Drug by Using the Quality by Design Approach. *Chem. Pharm. Bull.* **2017**, *65*, 218–228, https://doi.org/10.1248/cpb.c16-00415.
40. Alper Öztürk, A.; Namll, I.; Aygül, A. Cefaclor Monohydrate-Loaded Colon-Targeted Nanoparticles for Use in COVID-19 Dependent Coinfections and Intestinal Symptoms: Formulation, Characterization, Release Kinetics, and Antimicrobial Activity. *Assay Drug Dev. Technol.* **2021**, *19*, 156–175, https://doi.org/10.1089/adt.2020.1014.
41. Zeeshan, M.; Ali, H.; Ain, Q.U.; Mukhtar, M.; Gul, R.; Sarwar, A.; Khan, S. A holistic QBD approach to design galactose conjugated PLGA polymer and nanoparticles to catch macrophages during intestinal inflammation. *Mater. Sci. Eng. C* **2021**, *126*, 112183, https://doi.org/10.1016/j.msec.2021.112183.
42. Ismail, R.; Sovány, T.; Gácsi, A.; Ambrus, R.; Katona, G.; Imre, N.; Csóka, I. Synthesis and Statistical Optimization of Poly (Lactic-Co-Glycolic Acid) Nanoparticles Encapsulating GLP1 Analog Designed for Oral Delivery. *Pharm. Res.* **2019**, *36*, 99, https://doi.org/10.1007/s11095-019-2620-9.
43. Rajpoot, K.; Tekade, R.K. Chapter 10 - Microemulsion as drug and gene delivery vehicle: an inside story. In Drug Delivery Systems; Academic Press, **2019**, 455–520, https://doi.org/10.1016/B978-0-12-814487-9.00010-7.
44. Jena, G.K.; Patra, C.N.; Panigrahi, K.C.; Sruti, J.; Patra, P.; Parhi, R. QbD enabled optimization of solvent shifting method for fabrication of PLGA-based nanoparticles for promising delivery of Capecitabine for antitumor activity. *Drug Deliv. Transl. Res.* **2022**, *12*, 1521–1539, https://doi.org/10.1007/s13346-021-01042-0.
45. Scicluna, M.C.; Vella-Zarb, L. Evolution of Nanocarrier Drug-Delivery Systems and Recent Advancements in Covalent Organic Framework-Drug Systems. *ACS Appl. Nano Mater.* **2020**, *3*, 3097–3115, https://doi.org/10.1021/acsanm.9b02603.
46. Khan, F.U.; Nasir, F.; Iqbal, Z.; Neau, S.; Khan, I.; Hassan, M.; Iqbal, M.; Ullah, A.; Khan, S.I.; Sakhi, M. Improved Ocular Bioavailability of Moxifloxacin Hcl Using Plga Nanoparticles: Fabrication, Characterization, *In-vitro* and *In-vivo* Evaluation. *Iran. J. Pharm. Res.* **2021**, *20*, 592–608, https://doi.org/10.22037/IJPR.2021.114478.15054.
47. Panigrahi, D.; Sahu, P.K.; Swain, S.; Verma, R.K. Quality by design prospects of pharmaceuticals application of double emulsion method for PLGA loaded nanoparticles. *SN Appl. Sci.* **2021**, *3*, 638, https://doi.org/10.1007/s42452-021-04609-1.
48. Mehrotra, A.; Pandit, J.K. Critical Process Parameters Evaluation of Modified Nanoprecipitation Method on Lomustine Nanoparticles and Cytostatic Activity Study on L132 Human Cancer Cell Line. *J. Nanomed. Nanotechnol.* **2012**, *3*, 149, https://doi.org/10.4172/2157-7439.1000149.
49. Kesharwani, P.; Md, S.; Alhakamy, N.A.; Hosny, K.M.; Haque, A. QbD Enabled Azacitidine Loaded Liposomal Nanoformulation and Its in Vitro Evaluation. *Polymers* **2021**, *13*, 250, https://doi.org/10.3390/polym13020250.